In Silico Exploration of Bisphosphonate Scaffolds as Potential Inhibitors of SARS-CoV-2 RdRp for COVID-19 and PASC

Muzaffar-Ur-Rehman Mohammed [1,‡], Kishore Suryakant Chougule [1,‡], Chandu Ala, [1], Pranali Vijaykumar Kuthe [1], Mohit Garg [2], Murugesan Sankaranarayanan [1,*] and Seshadri S. Vasan [3,4,*]

[1] Department of Pharmacy, Birla Institute of Technology and Science, Pilani 333031, India
[2] Department of Chemical Engineering, Birla Institute of Technology and Science, Pilani 333031, India
[3] School of Medical and Health Sciences, Edith Cowan University, Joondalup, WA 6027, Australia
[4] Department of Health Sciences, University of York, York YO10 5DD, UK
[*] Correspondence: murugesan@pilani.bits-pilani.ac.in or prof.vasan@york.ac.uk
[‡] These authors contributed equally to this work.

Abstract: The novel coronavirus disease (COVID-19) pandemic has resulted in over 720 million confirmed cases and 7 million deaths worldwide, with insufficient treatment options. Innumerable efforts are being made around the world for faster identification of therapeutic agents to treat the deadly disease. Postacute sequelae of SARS-CoV-2 infection or COVID-19 (PASC), also called Long COVID, is still being understood and lacks treatment options as well. A growing list of drugs are being suggested by various *in silico, in vitro* and *ex vivo* models, however currently only two treatment options are widely used: the RNA-dependent RNA polymerase (RdRp) inhibitor remdesivir, and the main protease (M^Pro) inhibitor nirmatrelvir in combination with ritonavir. Computational drug development tools and *in silico* studies involving molecular docking, molecular dynamics, entropy calculations and pharmacokinetics can be useful to identify new targets to treat COVID-19 and PASC, as shown in this paper. We have investigated bisphosphonates which can bind competitively to nidovirus RdRp-associated nucleotidyl (NiRAN) transferase domain, and systematically down selected three candidates (CHEMBL196676, CHEMBL164344, and CHEMBL4291724) that show sufficient *in silico* promise to warrant further investigation in *in vitro* and *ex vivo* models.

Keywords: Bisphosphonates; Long COVID; MM-GBSA; Molecular docking; Molecular dynamics; RdRp; SARS-CoV-2; Virtual screening

1. Introduction

Coronaviruses are responsible for causing seasonal respiratory tract infections (RTIs) in people and are associated with common cold symptoms [1]. The highly pathogenic human coronaviruses (HCoVs) such as severe acute respiratory syndrome (SARS) associated coronavirus (SARS-CoV), Middle East respiratory syndrome–related coronavirus (MERS-CoV) and the novel SARS-CoV-2 cause infection to epithelial cells of the bronchi and pneumocytes, which could lead to life-threatening lung injuries [2]. Among these three, the SARS-CoV-2 virus which emerged in December 2019 exhibits faster human-to-human transmission, and resulted in over 780 million confirmed cases and 7 million reported deaths due to the novel coronavirus disease (COVID-19) [3]. Long COVID, also known as postacute sequelae of SARS-CoV-2 infection or COVID-19 (PASC) [4,5], may affect typically 3.1% of the population, especially those aged 35 to 69 years, females, people living in more deprived areas, those working in social care, those aged 16 years or over who were not working and not looking for work, and those with another activity-limiting health condition or disability [6].

SARS-CoV-2 employs a multi-subunit machinery for replication and transcription. Non-structural proteins (Nsp's) produced as cleavage products due to the open reading frame 1a and 1b (ORF1a and ORF1b) facilitate viral replication and transcription [7]. One of these, known as Nsp12 or RNA-dependent RNA polymerase (RdRp), catalyzes the synthesis of viral RNA and plays a central

role in the replication and transcription cycle of SARS-CoV-2 with Nsp7 and Nsp8 as co-factors [8,9]. Therefore, Nsp12 is considered a primary target for antiviral agents, with the potential for treating COVID-19 [10], and possibly other coronaviral diseases because it is a highly conserved motif. For example, sequence alignment results from the literature shows 96% common identity between SARS-CoV and SARS-CoV-2 [11].

In this work, as we shall be using RdRp as a key target let us first describe its components: it has the Nsp12 catalytic subunit, two accessory subunits (Nsp8 and Nsp7), and more than two turns of RNA template-product duplex [12]. The RdRp domain is analogous to a cupped right hand, consisting of the finger 'F' (amino acid residues 398–581, 628–687), palm (amino acid residues 582–627, 688–815) and thumb (amino acid residues 816–919) subdomains found in all single-subunit polymerases [13]. An in-depth structural analysis depicts the Nsp12 subunit binding to the first turn of RNA between its F and thumb sub-domains. The core protein consists of a single chain of 942 amino acids. The active site comprises of five conserved Nsp12 elements that are found in the palm motif. The amino acids Asp760 and Asp761 (Figure 1) are necessary for synthesis, which binds to the 3' end of the RNA. The RNA template is positioned by the supplementary Nsp12 finger motif. The second turn is positioned by two copies of Nsp8 that bind to the cleft on the opposite sides. As RNA exits, large helical extensions of Nsp8 protrude and create positively charged sliding poles that are necessary for coronaviruses to replicate their lengthy genomes [14]. Structural stability requires two Zinc (Zn) ions interacting with the residues present in the N-terminal domain (His295, Cys301, Cys306, Cys310) and finger domain (Cys487, His642, Cys645, Cys646). The presence of Zn in this site indicates its crucial role in stabilizing the overall 3D structure of the protein [15]. The binding of drugs to the amino acid residues in motif F of RdRp results in the aversion of entry of the substrate and divalent cations into the central active site cavity, thereby inhibiting the catalytic activity of the enzyme and preventing the RNA replication [16].

So far, the standard drugs of choice for treatment have been the emergency use authorized (EUA) drugs, nirmatrelvir and remdesivir. Nirmatrelvir is an orally available main protease inhibitor [17], while remdesivir is an RdRp inhibitor that is administered parenterally. The EUA status of remdesivir was revoked on April 2022, and approval as a supplemental new drug application (sNDA) has been given in December 2022 [16]. However, a recent study published in *The Lancet* shows that while remdesivir could reduce the risk it had an insignificant effect in ventilated COVID-19 patients [17]. Nirmatrelvir, a main protease inhibitor, exhibited promising antiviral effects but was susceptible to rapid degradation. To mitigate this issue, ritonavir, a protease inhibitor, was incorporated in a combined formulation which received FDA approval as the first oral antiviral pill PAXLOVID [18]. Other drugs that have shown promise include molnupiravir [19], favipiravir [20] and fluvoxamine [21,22]. However, molnupiravir and favipiravir are no longer recommended as the former drug has poor clinical outcomes [23–25] and the latter showed ineffective in viral clearance [26–28]. Although fluvoxamine has been shown to have both immunomodulatory effects [29] as well as anti-viral effect [21,30,31], it is clear that this drug can only be used in combination and not in its own [21,29].

Therefore, the quest to identify potential molecules to treat COVID-19 and PASC is still ongoing [32]. In the literature, when databases of molecules including synthetic and natural origin were screened against RdRp [33–40] together with other non-structural proteins (Nsp's) [41–44] inhibitors, such studies suggest the use of natural substances as alternative to remdesivir. Few studies also reported the screening of analogues of different scaffolds such as quinolines [40], cytidines [45] and andrographolides [46]. Notably, drug repurposing efforts across the world have proposed several drugs that are yet to be tested *in vitro* [13,32,38–40,47–54]. As RdRp is a key target, this paper looks at a class of small molecules called bisphosphonates (BPs) for four reasons: 1. The use of BPs is associated with a significant three- to five-fold reduction in the incidence of SARS-CoV-2 testing, COVID-19 diagnosis, and COVID-19-related hospitalization during the pandemic [55]; 2. BP scaffolds exhibit competitive binding to the nidovirus RdRp-associated nucleotidyl (NiRAN) transferase domain [56]; 3. Our prior experience with an immunomodulatory drug, fluvoxamine in *in silico* and *ex vivo* studies [21]; and 4. Our recent study which has shown that alendronate, a BP drug, shows

more promising *in silico* results compared to remdesivir [32]. Therefore, we shall further explore BPs in detail as it is the focus of this follow-up study.

BPs are a class of small-molecule drugs that have two phosphonate groups. They are categorized into nitrogen-containing (amino-BPs) and nitrogen-free BPs (non-amino-BPs). They are mainly used to treat osteoporosis, Paget's disease of the bone, and to lower high calcium levels in people with cancer [57]. In addition, amino-BPs control the activation, expansion, and function of a significant portion of human γδT cells (i.e., it reduces the amount of circulation γδT cells), as well as neutrophils, monocytes and macrophages. They can also modify the dendritic cell's ability to present antigens to the immune system. Results from animal experiments indicate that both amino-BPs and non-amino-BPs have strong adjuvant-like effects of increasing antibody and T-cell responses to viral antigens. [58]. Acknowledging the range of immunomodulatory effects and their binding with RdRP inspired us to investigate these as prospective COVID-19 drug candidates [55,56,58].

2. Materials and Methods

In this study, a series of compounds having BPs were downloaded from the ChEMBL database [59] and molecular docking study was carried out to get all the "hit" molecules. These hits were further down-selected using molecular mechanics with generalized Born and surface area (MM-GBSA) studies and the top four ligands were analyzed for their dynamic behavior via molecular dynamics studies followed by the entropic calculations using the software "gromacs" (v2022.4).

2.1. Protein Preparation

While the literature shows a high sequence identity (96%) between the RdRp proteins of SARS-CoV and SARS-CoV-2, we couldn't find any report with MERS-CoV, so the latter's RdRp domain (residues 4845–5412 from accession code A0A023YA54) was taken and multiple sequence alignment was carried out to reveal the conserved motifs (75%) for these three coronaviruses (Figure 1). Further, to provide a valuable starting point for BPs screening against SARS-CoV-2, RdRp protein (PDB: 6M71) [8] was selected and downloaded from the protein data bank (https://www.rcsb.org/). The protein was prepared using the protein preparation wizard of the glide module of the Schrödinger software (Schrödinger LLC., NY, v2022) [60]. Missing hydrogens and residues were added using the software's prime module and pre-processed using the Epik module at pH 7.0±2.0 [61]. The protein was optimized by removing water molecules beyond 3 Å and subjected to minimization using the optimized potentials for liquid simulations 4 (OPLS4) force field [61].
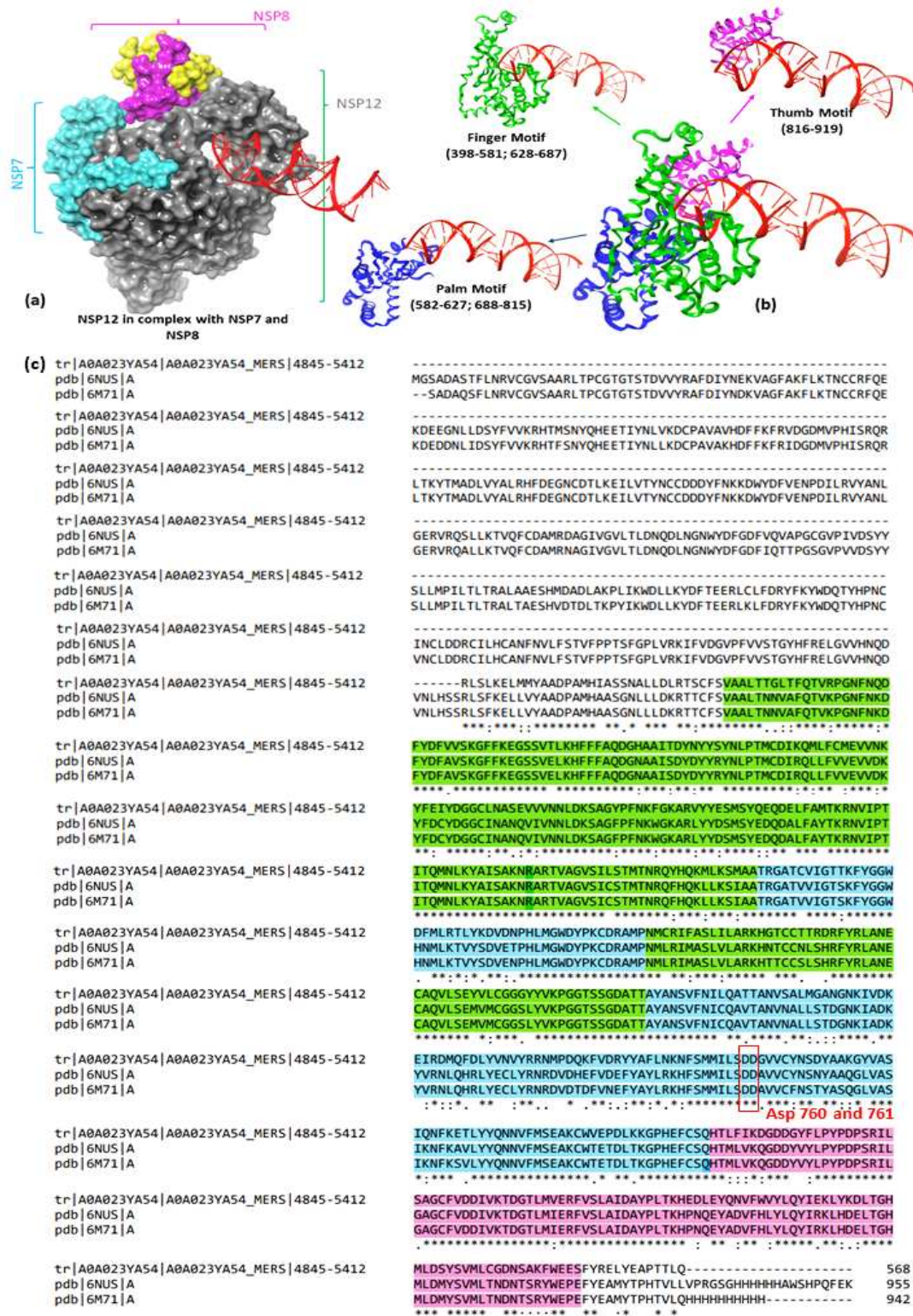
Figure 1. Structure of RdRp representing (a) Nsp 12 in complex with Nsp 7 and Nsp 8; (b) ribbon form representation of the Nsp 12 with different motifs; (c) the RdRp sequence alignment of MERS, SARS and SARS-CoV-2 representing the motifs highlighted in green, blue, and pink colors. The alignment shows highly conserved regions (*) among the three viruses (75%); the residues Asp760-761 are also conserved as they are essential for RNA synthesis.

2.2. Ligand preparation

ChEMBL database has been used to download molecules containing BPs based on the Tanimoto similarity check (95%) [44]. These molecules were imported and prepared using Ligprep module of maestro (Schrödinger LLC., NY, v2022)). The ionization state was set to neutral and chirality was determined from the 3D structure. The force field OPLS4 was employed to prepare the ligands.

2.3. Molecular docking

For carrying out molecular docking studies, a grid box of 10 Å^3 was generated using the maestro receptor grid generation wizard (Schrödinger) by specifying the binding (active) site residue Arg555 as no co-crystal ligand was available [49]. The ligands were docked using the ligand docking wizard of the glide module of Schrödinger with standard-precision (SP) mode initially. The molecules that were able to bind were subjected to filtration by applying the criterion of molecular weight (<500 Da) and number of rotatable bonds (<10) [63]. Molecules obtained from this filtration process were then subjected to docking with extra-precision (XP) mode [64].

2.4. MM-GBSA calculations

Molecular mechanics with generalised Born and surface area solvation (MM-GBSA) studies help to calculate the ligand's binding-free energy (ΔG_{bind}) value. The calculations were mainly based on the summation of differences in the minimization (ΔE_{MM}), solvation (ΔG_{Solv}), and surface area ($\Delta G_{S.A.}$) energies of RdRp-ligand complex structure and free RdRp and ligand molecules [65]. The protein-ligand complex (PLC) from the docking studies was used to calculate the binding free energy. The analysis was carried out in the prime module of Schrödinger software. OPLS4 force field with dielectric surface generalized Born (VSGB) continuum solvation model was used. Based on the following formula, the binding free energy of the ligand was calculated:

$$\Delta G_{bind} = \Delta E_{MM} + \Delta G_{solv} + \Delta G_{SA} \dots\dots\dots\dots\dots\dots\dots\dots\dots\dots (1)$$

2.5. Molecular dynamics studies

The molecular dynamics (MD) simulation was accomplished to determine the ligand molecules' stability, confirmation and intermolecular interaction with the target RdRp protein (PDB ID: 6M71) [66]. The time-dependent modification of the complexes was estimated over 100 ns using the Desmond module. The MD simulation was executed under thermodynamic conditions (applied volume, density, pressure and temperature). The complete system was annealed and equilibrated using ensembles.

The down-selected ligand complexes were imported and prepared using the protein preparation wizard of the Desmond module (Schrödinger LLC., NY, v2020)). The complex was solvated using the transferable intermolecular potential with 3 points (TIP3P) model and the grid boundary dimensions was set to 10 Å^3 [67]. The complex model was electrically neutralized with Na$^+$/Cl$^-$ ions, and built using a system builder wizard. The complete solvated model was minimized and molecular dynamics was carried out for 100 ns on all five selected complexes (including the reference drug remdesivir). The root means square deviation (RMSD), root mean square fluctuation (RMSF) and interaction plots were used to interpret the stability of appropriate complexes.

2.6. Entropy calculation for molecular dynamics trajectories

The binding free energy of the protein-ligand complex was determined using the gmx_mmPBSA tool [68,69]. In this calculation, the Poisson-Boltzmann surface area (PBSA) method with a dielectric model (ipb = 2) and a non-polar solvation model (inp = 1) were employed. The ionic strength of the surrounding medium was maintained at 0.15 M, and the temperature was set at 310 K. To calculate the entropy (-TΔS), the interaction entropy (I.E.) method was used [70]. This allowed us to evaluate the change in binding free energies with entropy contributions for the protein, ligand, and their complexes. The trajectories from the protein-ligand MD simulation in explicit water from the
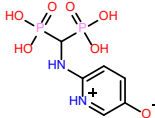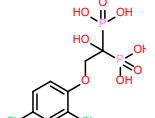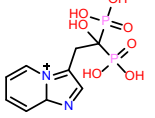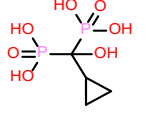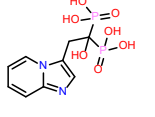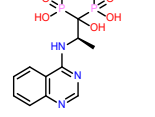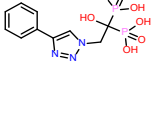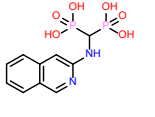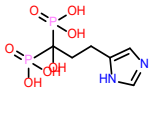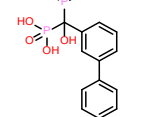
Desmond module were used to generate the gromacs trajectory file required for calculations using visual molecular dynamics (VMD) software.
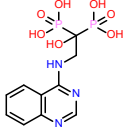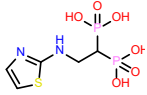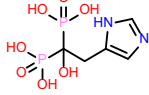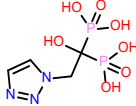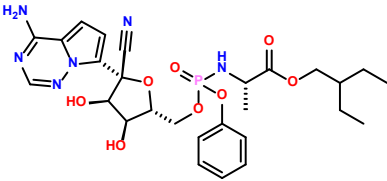
Additionally, topology files for protein and ligand were obtained separately by converting the *.cms files to *.gro and *.top files using the intermol software [71]. Since the initial frames during the dynamic simulation are involved in the equilibrium, the frames after 50 ns were considered for analysis data. To speed up the procedure and to get better averaging, we ran five independent MMPBSA calculations (10 ns each) for every complex from 50-100 ns and reported the average and standard deviation of these calculations [72].

3. Results and Discussion

All the drug molecules (synthetic and approved) obtained from the ChEMBL database were docked into the binding site of the RdRP protein (PDB ID: 6M71) using the ligand docking wizard of the glide module of Schrödinger software. The test molecules were docked using SP mode and we obtained 1992 molecules, signifying that all test molecules have occupied the active site pocket. Larger molecules >500 Daltons find it harder to absorb as smaller molecules are more absorbable. Hence, we used a molecular weight (<500 Daltons) filter to filter out large molecules. The number of drugs that passed the filter was 1398, leaving behind 594 molecules. To further reduce the number of molecules, a filter corresponding to the number of rotatable bonds (<10) was applied, as the drugs having fewer rotatable bonds are acceptable (<10) [73][63]. With this filter, six hundred twenty-eight (628) molecules were obtained, which were further subjected to molecular docking using extra precision (XP) mode. All the molecules were binding to the active site with varying glide scores; hence, a cut-off score of -9.0 kcal/mol was considered to down-select the compounds. The list of molecules obtained after the cut-off is shown in Table 1.

Table 1. Molecular docking results of top 14 bisphosphonate ligands.

S. No	ChEMBL ID	Structure	Docking score kcal/mol	S. No	ChEMBL ID	Structure	Docking score kcal/mol
1	CHEMBL121326 5		-10.235	8	CHEMBL164344		-9.213
2	CHEMBL608526		-9.706	9	CHEMBL300361		-9.151
3	CHEMBL319144		-9.657	10	CHEMBL428999 6		-9.119
4	CHEMBL480297 1		-9.355	11	CHEMBL387132		-9.11
5	CHEMBL98211		-9.347	12	CHEMBL196676		-9.059

6	CHEMBL429172 4		-9.308	13	CHEMBL456930 8		-9.02
7	CHEMBL301247		-9.219	14	CHEMBL338622		-9.014
15	Remdesivir (Reference drug)						-3.270

3.1. MM-GBSA studies

These top 14 molecules obtained using a cut-off value of <-9.0 kcal/mol from molecular docking studies were subjected to MM-GBSA studies to evaluate the binding free energy of the ligand, and the molecules with the least score when compared to remdesivir were selected. The binding energy of remdesivir was found to be -40.32 kcal/mol, and we see that four molecules have lower binding energy. The 14 molecules (Table 2) were divided into three categories, i.e., low, moderate, and high binding energy, with 6, 4 and 4 each. As the last category of molecules showed the least energy compared to remdesivir, we further analyzed their interaction pattern (depicted in Figure 2 and Table 3) and extrapolated our study using these molecules for molecular dynamics studies.

Table 2. MM-GBSA scores of the top-hit bisphosphonate ligands.

S. No	Category	Drugs	MM-GBSA dG Bind (Kcal/mol)
1.	High binding energy	CHEMBL1213265	-7.74
		CHEMBL338622	-24.14
		CHEMBL301247	-24.22
		CHEMBL4289996	-24.81
		CHEMBL98211	-26.04
		CHEMBL300361	-26.68
2.	Moderate binding energy	CHEMBL608526	-33.42
		CHEMBL319144	-35.2
		CHEMBL4802971	-36.77
		CHEMBL4569308	-40.94
3.	Low binding energy	CHEMBL4291724	-41.51
		CHEMBL387132	-43.28
		CHEMBL196676	-44.14
		CHEMBL164344	-46.65
4.	**Reference ligand**	**Remdesivir**	**-40.32**
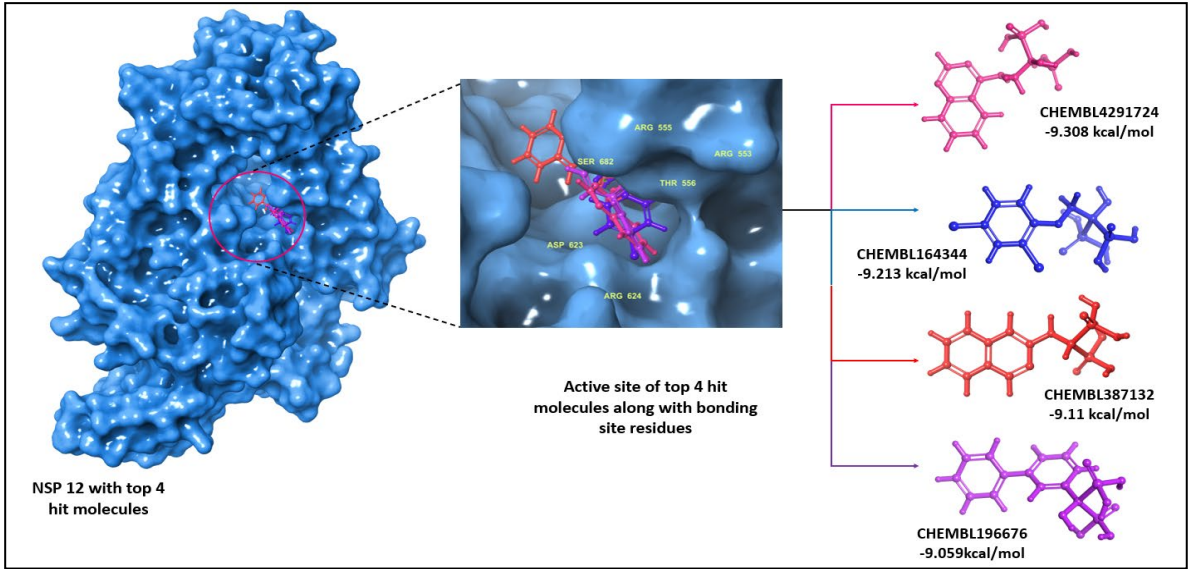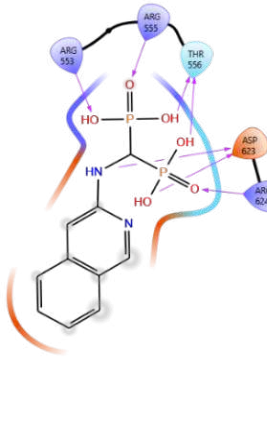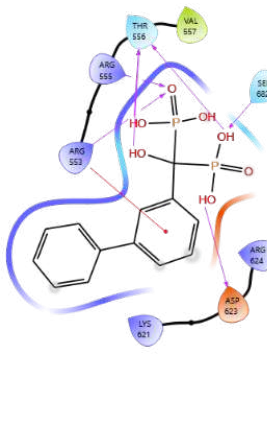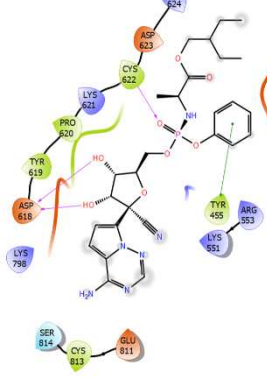
Figure 2. Top 4 hit molecules with target protein Nsp12 along with docking score.

Table 3. Amino acid interactions of top four bisphosphonate ligands.

S. No	ChEMBL ID	2D Interaction Diagram	Docking Score	Interacting residue	Interaction type	Bond Length (Å)
1	CHEMBL4291724		-9.308	Thr556	H-Bond	1.61, 1.92
				Asp623	H-Bond	1.57
				Arg553	H-Bond	1.91
				Arg555	H-Bond	2.69, 2.22
				Arg624	H-Bond	2.40
2	CHEMBL164344		-9.213	Thr556	H-Bond & X-Bond	1.62, 1.68 & 3.21, 3.06
				Asp623	H-Bond	1.59
				Arg553	H-Bond	2.16
				Arg555	H-Bond	2.08, 2.16
				Arg624	H-Bond & X-Bond	2.60 & 2.96
3	CHEMBL387132		-9.11	Thr556	H-Bond	2.01, 1.62

		Structure		Residue	Interaction	Distance
				Asp623	H-Bond	1.67, 1.79
				Arg555	H-Bond	2.44
				Arg553	H-Bond	1.88, 2.01
				Arg624	H-Bond	2.05
4	CHEMBL196676		-9.059	Thr556	H-Bond	2.12, 1.71, 1.79
				Ser682	H-Bond	1.82
				Arg555	H-Bond	2.17, 1.89
				Asp623	H-Bond	1.62
				Arg553	H-Bond	2.23
5.	Remdesivir		-3.270	Tyr455	π-π stacking	5.34
				Asp618	H-bond	1.81, 1.98
				Cyc622	H-bond	2.66

3.2. Molecular dynamics results

The top ligands with the least binding energy from MM-GBSA studies were analyzed by molecular dynamics studies (Figure 3). The clinically used drug remdesivir was also subjected to dynamics simulations for comparative analysis, and showed a stable RMSD plot for the entire duration (5.0 Å-7.0 Å from the initial 5 ns until the end). Additionally, the fluctuations in the active site region of the protein were low, resulting in a stable RMSD and RMSF plots of the protein (Figures 3 and 4). During this, significant interactions were observed by the residues of the palm domain that are necessary to bind with the RNA. The residual interactions include Asp618 (63%, water-mediated), Asp623 (70%, water-mediated), and Asp760 (90%, H-bond) (Figure 5). In the case of compound CHEMBL164344, the RMSD plot has deviations till 10.0Å for the initial 18 ns, during which strong interactions were observed with the residues of palm domain, Thr556, Asp623, and Arg624; later, these interactions gradually decreased, and the interactions with two residues of F domain, Asp452 (81%, H-bond) and Tyr455 (61%, π-π stacking) increased over the time. This has caused a decrease in the RMSD from 12.0 Å at 20th ns to 7.5 Å at 100th ns. Change of phenoxymethyl (as in CHEMBL164344)

with biphenyl group (as in CHEMBL196676) results in significantly more interactions with the residues Asp452 (81%, H-bond) of F domain and Asp623 (85%, H-bond) of palm domain, as well as inconsistent water-mediated interactions with Asp760 (27%) (Figure 5). Initially, the interactions with Arg553, Thr556, and Asp623, as observed in the docked complex, remained for 18 ns, during which no significant deviations were observed (RMSD between 1.0 Å – 3.0 Å); later, the interactions with Asp452, Lys621 along with Asp623 had changed the ligand's conformation, resulting in the increase in the RMSD ranging between 8.0 Å and 7.0 Å which retained till 70 ns, and then a gradual decrease until the end of the simulation (last frame RMSD is 5.4 Å) (Figure 3). The N-methyl quinazoline-4-amine compound (CHEMBL4291724) shows greater stability in terms of its RMSD plot as equilibrium is attained after 20 ns until the end of the simulation with RMSD ranging between 10.0 Å and 12.0 Å (Figure 3). Most of the interactions are between the phosphonic acid groups and the residues of the palm domain, which include Asp623, Thr680, and Asp760, with a contribution of 50%, 39%, and 86%, respectively (Figure 5). In the case of CHEMBL387132, the RMSD plot is comparatively lower than all other complexes, as the overall deviations for 100 ns were between 3.0 Å and 6.4 Å. Additionally, strong interactions were observed with Asp623 for the first 30 ns and then with Asp760 of the palm domain, contributing to an overall interaction of 30% and 64%, respectively. A residue from the F domain, Lys545, has a total of 33% H-bond interactions with the ligand. (Figures 3 and 5). The protein RMSD plot shows a similar pattern of deviations with all the hit ligands, indicating their stability with the ligands during the MD simulation. Similarly, the RMSF plot shows that interacting residues in the active site have acceptable fluctuations (<2.0 Å) (Figure 4). From this, we infer that the selected top ligands behave in a similar fashion to that of remdesivir, with the active site residues forming strong bonds, and most of the interactions by our "hit compounds" attributable to bisphosphonic acid groups. Therefore, there is a high probability that these compounds may emerge as potential RdRp inhibitors if evaluated *in vitro*.
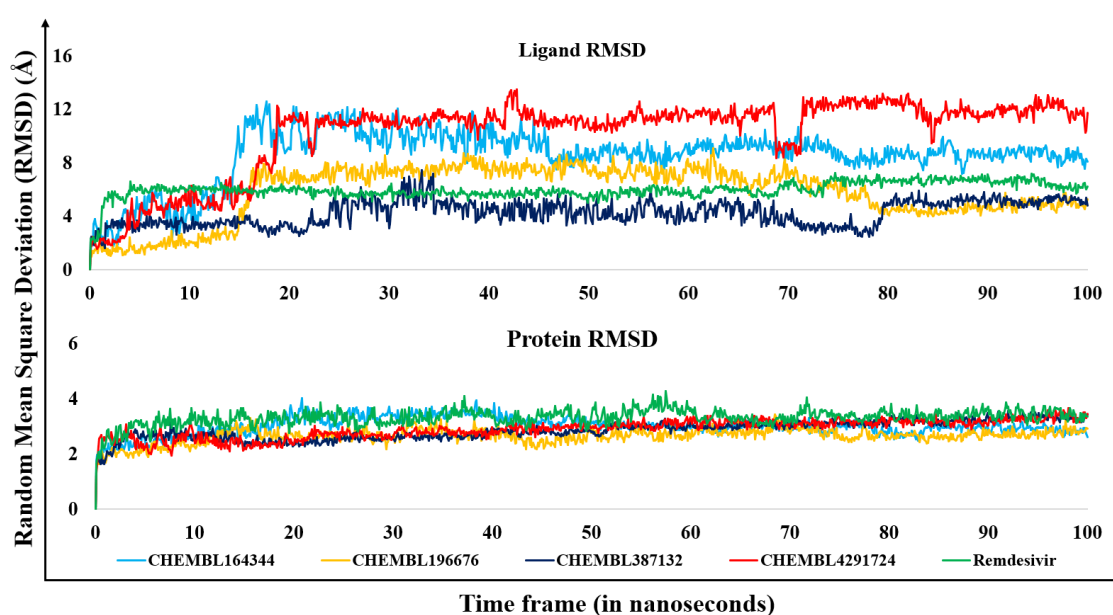
Figure 3. RMSD plot of the 4 hit ligands (above) and the protein (PDB ID: 6M71).
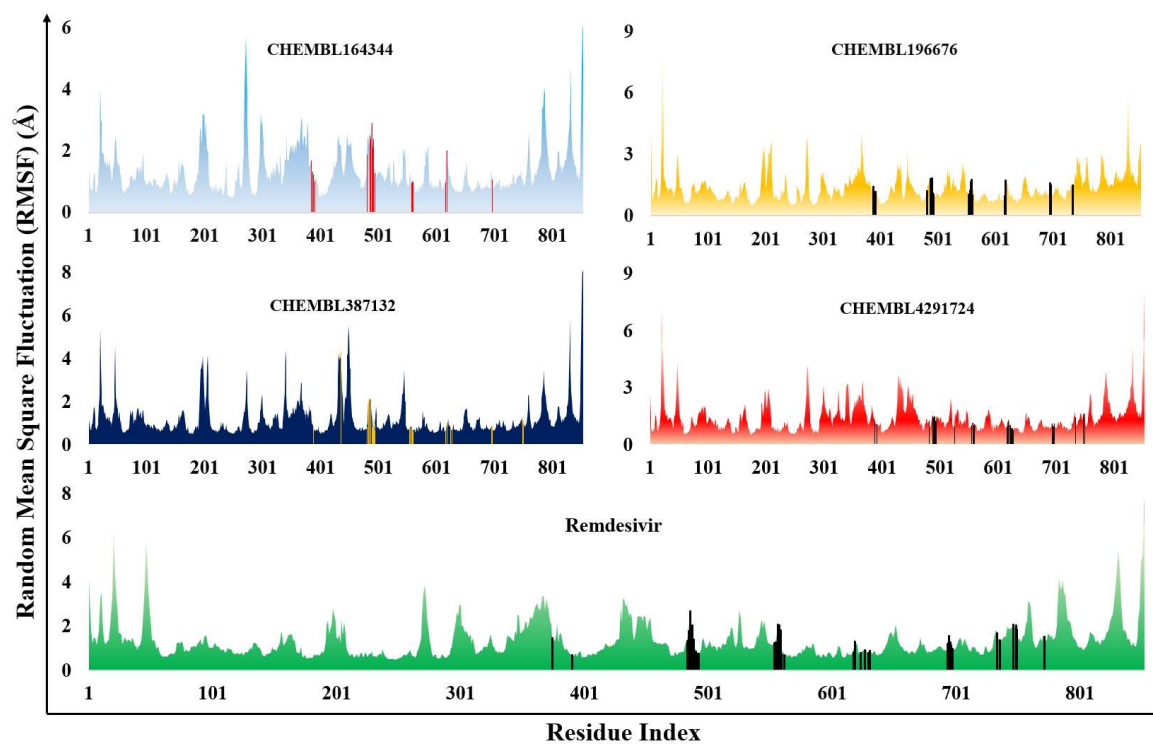
Figure 4. RMSF plot of 6M71 corresponding to the top 4 bisphosphonate ligands and reference drug (remdesivir). The fluctuations are shown in colored area plot, while the H-bond interactions are shown as histogram plot within the area.
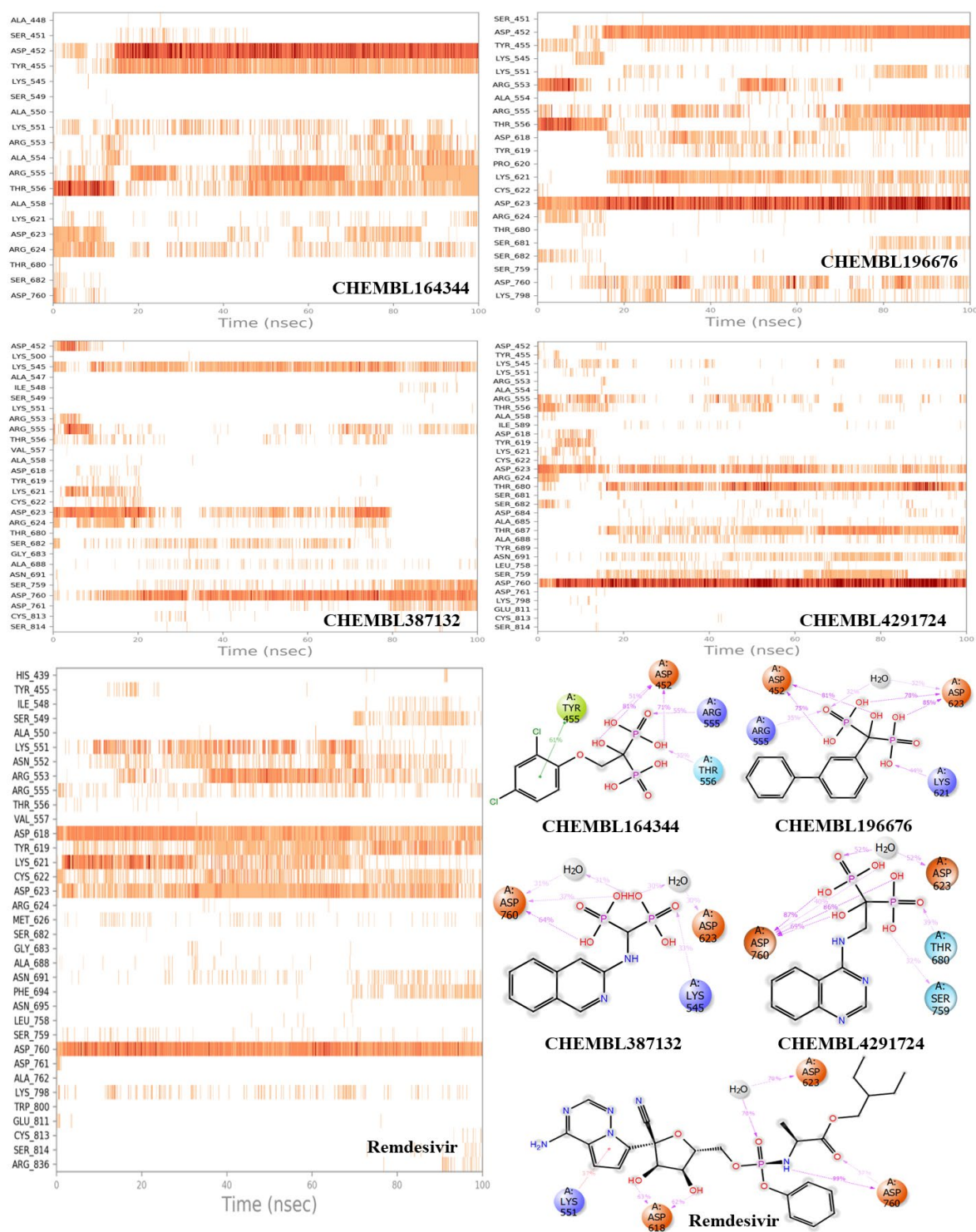
Figure 5. Protein-ligand contact plots of the top 4 bisphosphonate ligands showing timeline representation of contacts and individual residual contributions during the simulation.

3.3. Estimation of entropic contribution by gmx_MMPBSA

The molecular mechanics Poisson-Boltzmann surface area (MM/PBSA) analysis helps to understand entropic contribution between protein and ligand during the molecular dynamic simulations [74]. It refers to the degree of randomness in a system and can guide to understand the entropic contributions of the ligand in the active site of the protein. Since MMPBSA analysis module is not available in Schrödinger software, the gmx_MMPBSA tool was used to determine the entropic

contributions of the ligands, protein, and the protein-ligand complexes [68]. The change in free energy (ΔG) of the complex is then calculated using the following equation:

$$\Delta G_{binding} = G_{complex} - \left(G_{protein} + G_{ligand}\right) \quad \dots\dots\dots\dots\dots\dots\dots \ (2)$$

In the above equation (1), the $G_{binding}$ represents the free energy of the protein-ligand complex in water, while $G_{protein}$ and G_{ligand} represent the free energies of the protein and ligand respectively in water. The free energy of the total system ($\Delta G_{binding}$) can be obtained by subtracting the interaction entropy (I.E.) from the change in total energy (ΔE_{MM}) of the system. ΔE_{MM} is the summation of various change in energies such as van der Waals (ΔE_{vdw}), electrostatic columbic (ΔE_{EL}), electrostatic potential (ΔE_{PB}) and non-polar (ΔE_{NPOLAR}).

$$\Delta G_{binding} = (\Delta E_{MM} - T\Delta S) \dots\dots\dots\dots\dots\dots\dots\dots\dots\dots\dots \ (3)$$

Whereas, $\Delta E_{MM} = (\Delta E_{vdw} + \Delta E_{EL} + \Delta E_{PB} + \Delta E_{NPOLAR}) \dots\dots\dots\dots. \ (4)$

Applying equation (3), the free energy of the systems ($\Delta G_{binding}$) was calculated and tabulated in Table 4. From the results, it is clear that the compound CHEMBL196676 had entropy contributions less than remdesivir as their interaction entropies (I.E.) were 9.476 kcal/mol and 10.856 kcal/mol respectively, whereas, their $\Delta G_{binding}$ were -33.404 kcal/mol and -19.914 kcal/mol respectively. The higher negative values indicate the free energy of the complex is lower than the sum of individual free energies of the protein and ligand. Similarly, the I.E. values in the case of CHEMBL164344 (13.764 kcal/mol) and CHEMBL4291724 (15.428 kcal/mol) were slightly greater than remdesivir, however, due to lower total energy (ΔE_{MM}) the binding free energies were better than remdesivir (Figure 6). The compound CHEMBL387132 shows higher I.E. and ΔE_{MM} values, resulting in poor binding free energy. These results are in agreement with our molecular dynamics studies wherein the 4 hit compounds showed significant interactions with the active site residues except for CHEMBL387132.

Table 4. Entropy results of the top hit compounds showing the entropy contributions, total energies of the system, and the total binding free energies of the ligand at different time frames.

Compounds	I.E.	Total energy contributions (ΔE_{MM})					$\Delta G_{binding}$
		ΔE_{VDW}	ΔE_{EL}	ΔE_{PB}	ΔE_{NPOLAR}	$\Delta E_{MM} = \sum \Delta E$	
CHEMBL164344	13.76	-22.77	-93.71	79.14	-3.19	-40.53	-26.77
CHEMBL196676	9.48	-13.06	-90.55	63.70	-2.98	-42.88	-33.41
CHEMBL4291724	15.43	-13.47	-123.47	97.86	-2.73	-41.81	-26.38
CHEMBL387132	20.52	-20.15	-87.58	88.93	-2.88	-21.68	-1.16
Remdesivir	10.86	-52.27	-64.85	92.31	-5.95	-30.77	-19.91

I.E. = Interaction entropy; ΔE_{MM} = Total energy contributions of the system; ΔG = binding free energy
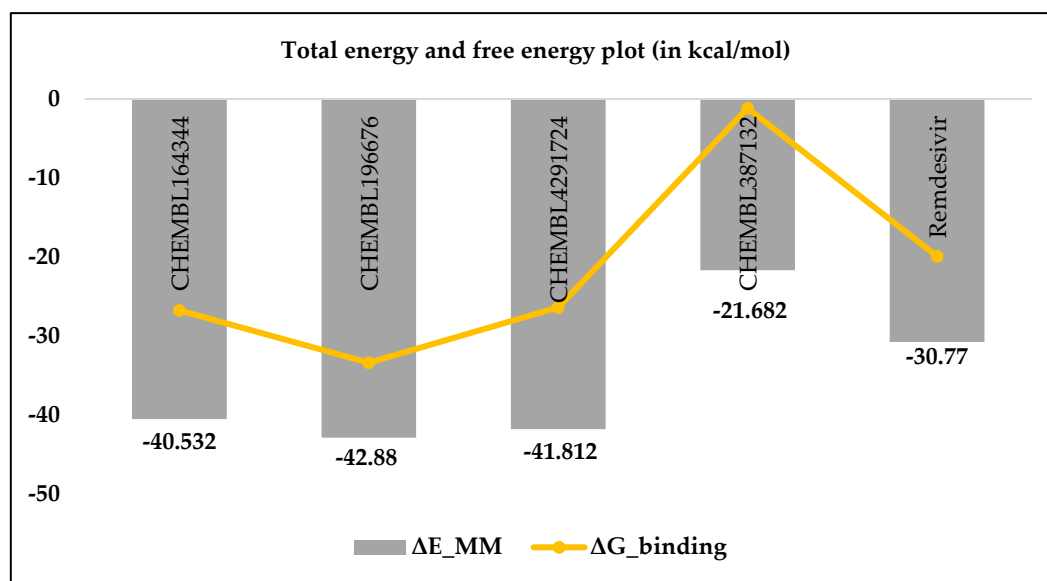
Figure 6. Free energy plot showing the total energies of the system (histogram) and the binding free energies of the hit compounds (line graph) during the dynamics simulations.

3.4. *Results of in silico predicted ADMET profiles*

This study estimated the pharmacokinetic and toxicological predictions of the top-hit BP molecules. The predicted results showed satisfactory results for three compounds (CHEMBL4291724, CHEMBL387132, CHEMBL196676). The compound CHEMBL164344 showed a low Caco-2 permeability score, and the intestinal absorption is <30%, indicating the compound may have a low absorption profile. The other three compounds exhibited similar skin permeability; none acted as a P-glycoprotein (P-gp) substrate. The drug that acts as a substrate to P-gp showed low bioavailability, as evident from the studies of remdesivir [54]. The volume of distribution in steady state condition (Vd_{ss}) for all the compounds is less except for CHEMBL196676, which possessed better tissue distribution value than remdesivir. The fraction of the drug that remains unbound with blood plasma protein is essential to pass through cell membranes; therefore, the higher the fraction unbound (Fu) value, the higher its distribution [75]. All four compounds have better Fu values than the reference drug (0.005 Fu). Due to the presence of phosphonate groups, the compounds are likely to have poor permeability to the blood-brain barrier (BBB) or the central nervous system (CNS); however, CHEMBL387132 and CHEMBL196676 exhibited better permeability profiles than remdesivir. None of the molecules are likely to be metabolized by cytochrome P450, and all showed a better clearance rate. The maximum tolerated dose is higher than remdesivir and does not inhibit the human ether-a-go-go gene (hERG). The rat oral toxicity levels are higher than remdesivir, indicating high concentrations are required to cause toxicity. The other toxicity parameters are better compared to remdesivir (Table 5).

Table 5. Results of in silico predicted ADMET profiles of hit bisphosphonate molecules.

Parameters		Hit molecules				
	CHEMBL →	4291724	164344	387132	196676	Remdesivir
Absorption	WS (log mol/L)	-2.47	-2.152	-2.046	-3.677	-3.07
	CP (log Papp in 10^{-6} cm/s)	-0.438	-0.461	0.093	1.245	0.635
	IA (% Absorbed)	42.008	16.774	71.627	38.34	71.109
	S.P. (log Kp)	-2.735	-2.743	-2.759	-2.735	-2.735
	P-gly Substrate	No	No	No	No	Yes

		Inhibitor	I	No	No	No	No	Yes
			II	No	No	No	No	No
Distribution		V.D. ss (log L/kg)		-0.768	-0.558	-0.814	0.578	0.307
		FU (Fu)		0.331	0.469	0.516	0.028	0.005
		BBB (log BB)		-2.302	-2.284	-1.86	-1.908	-2.056
		CNS (log P.S.)		-4.756	-3.881	-4.034	-3.879	-4.675
Metabolism	CYP action	Substrate	2D6	No	No	No	No	No
			3A4	No	No	No	No	Yes
		Inhibition against 1A2, 2C19, 2C9, 2D6, 3A4		No for all four molecules				
Excretion		T.C. (log ml/min/kg)		0.146	0.032	-0.025	-0.119	0.198
		ROC		No	No	No	No	No
Toxicity		AMES		No	No	No	Yes	No
		MTD (log mg/kg/day)		0.841	0.445	0.689	0.574	0.15
		hERG I inhibitor		No	No	No	No	No
		hERG II inhibitor		No	No	No	Yes	Yes
	Rat oral toxicity	Acute (LD_{50}) (mol/kg)		2.67	2.613	1.886	3.117	2.043
		Chronic (LOAEL) (Log mg/kg_bw/day)		3.195	3.597	3.052	3.404	1.639
		HT		Yes	No	Yes	No	Yes
		SS		No	No	No	No	No
		TT (log ug/L)		0.285	0.285	0.288	0.285	0.285
		MT (log mM)		2.992	1.686	2.938	0.427	0.291

W.S.: Water Solubility, CP: Caco2 permeability, IA: Intestinal absorption (human), S.P.: Skin Permeability, V.D. ss: Volume of distribution in steady state, F.U.: Fraction unbound (human), T.C.: Total Clearance, ROC: Renal OCT2 substrate, MTD: Max. Tolerated dose (human), LD_{50}: Lethal dose at 50% concentration, LOAEL: Lowest observed Adverse effect level, H.T.: Hepatotoxicity, S.S.: Skin Sensitization, TT: T. Pyriformis toxicity, MT: Minnow toxicity

4. Conclusions

In the current study, an *in silico* investigation of BP-containing molecules obtained from the CHEMBL database was carried out. The preliminary studies produced 14 compounds with the best docking score compared to remdesivir, but from MM-GBSA analysis, four molecules were observed to be better than remdesivir with superior molecular dynamics. The agreement between entropy and dynamics results, combined with *in silico* predicted ADMET analysis, lead us to predict that three of these compounds (CHEMBL196676, CHEMBL164344 and CHEMBL4291724) are suitable candidates for synthesis and *in vitro* evaluation against RdRp. These candidates also have better water solubility, Caco2 permeability, intestinal absorption, distribution, metabolism and excretion profiles. They have poor bioavailability and toxicity profile but are better than the reference drug, remdesivir, which is currently under clinical use.

Author Contributions: Conceptualization, M.M.U-.R., M.S., and S.S.V.; methodology, M.M.U-.R., C.K.S., A.C. and P.V.K..; software, P.V.K., R.P.J., S.R.J.; validation, M.M.U-.R., M.S., and S.S.V.; formal analysis, M.M.U-.R., C.K.S., A.C., and P.V.K.; investigation, C.K.S., R.P.J., S.R.J.; resources, M.S., and S.S.V.; data curation, M.M.U-.R., and C.K.S.; writing—original draft preparation, M.M.U-.R., and C.K.S.; writing—review and editing, M.M.U-

.R., M.S., and S.S.V.; visualization, M.M.U-.R., A.C. and M.S.; supervision, M.S., and S.S.V. All authors have read and agreed to the published version of the manuscript.

Funding: This research received no external funding.

Institutional Review Board Statement: Not applicable.

Informed Consent Statement: Not applicable.

Data Availability Statement: Any data not provided in this study will be shared upon request.

Acknowledgments: The authors are thankful to BITS-Pilani for providing the necessary facilities to conduct the research.

Conflicts of Interest: The authors declare no conflict of interest.

References

1. Mesel-Lemoine, M.; Millet, J.; Vidalain, P.-O.; Law, H.; Vabret, A.; Lorin, V.; Escriou, N.; Albert, M.L.; Nal, B.; Tangy, F. A Human Coronavirus Responsible for the Common Cold Massively Kills Dendritic Cells but Not Monocytes. *J. Virol.* **2012**, *86*, 7577–7587, doi:10.1128/jvi.00269-12.

2. Zhu, Z.; Lian, X.; Su, X.; Wu, W.; Marraro, G.A.; Zeng, Y. From SARS and MERS to COVID-19: A Brief Summary and Comparison of Severe Acute Respiratory Infections Caused by Three Highly Pathogenic Human Coronaviruses. *Respir. Res.* **2020**, *21*, 224, doi:10.1186/s12931-020-01479-w.

3. WHO Coronavirus (COVID-19) Dashboard. WHO Coronavirus (COVID-19) Dashboard With Vaccination Data. Available online: https://covid19.who.int/ (accessed on 2 November 2023).

4. Thaweethai, T.; Jolley, S.E.; Karlson, E.W.; Levitan, E.B.; Levy, B.; Mccomsey, G.A.; Mccorkell, L.; Nadkarni, G.N.; Parthasarathy, S.; Singh, U.; et al. Development of a Definition of Postacute Sequelae of SARS-CoV-2 Infection. *JAMA* **2023**, *329*, 1934–1946, doi:10.1001/jama.2023.8823.

5. Proal, A.D.; VanElzakker, M.B. Long COVID or Post-Acute Sequelae of COVID-19 (PASC): An Overview of Biological Factors That May Contribute to Persistent Symptoms. *Front. Microbiol.* **2021**, *12*, 1–24, doi:10.3389/fmicb.2021.698169.

6. Office for National Statistics (ONS) Prevalence of Ongoing Symptoms Following Coronavirus (COVID-19) Infection in the UK: 2 February 2023 Available online: https://www.ons.gov.uk/peoplepopulationandcommunity/healthandsocialcare/conditionsanddiseases/bulletins/prevalenceofongoingsymptomsfollowingcoronaviruscovid19infectionintheuk/2february2023 (accessed on 6 November 2023).

7. Naqvi, A.A.T.; Fatima, K.; Mohammad, T.; Fatima, U.; Singh, I.K.; Singh, A.; Atif, S.M.; Hariprasad, G.; Hasan, G.M.; Hassan, M.I. Insights into SARS-CoV-2 Genome, Structure, Evolution, Pathogenesis and Therapies: Structural Genomics Approach. *Biochim. Biophys. acta. Mol. basis Dis.* **2020**, *1866*, 165878, doi:10.1016/j.bbadis.2020.165878.

8. Gao, Y.; Yan, L.; Huang, Y.; Liu, F.; Zhao, Y.; Cao, L.; Wang, T.; Sun, Q.; Ming, Z.; Zhang, L.; et al. Structure of the RNA-Dependent RNA Polymerase from COVID-19 Virus. *Science* **2020**, *368*, 779–782, doi:10.1126/science.abb7498.

9. Malone, B.; Urakova, N.; Snijder, E.J.; Campbell, E.A. Structures and Functions of Coronavirus Replication–Transcription Complexes and Their Relevance for SARS-CoV-2 Drug Design. *Nat. Rev. Mol. Cell Biol.* **2021**, *23*, 21–39, doi:10.1038/s41580-021-00432-z.

10. Gangadharan, S.; Ambrose, J.M.; Rajajagadeesan, A.; Kullappan, M.; Patil, S.; Gandhamaneni, S.H.; Veeraraghavan, V.P.; Nakkella, A.K.; Agarwal, A.; Jayaraman, S.; et al. Repurposing of Potential Antiviral Drugs against RNA-Dependent RNA Polymerase of SARS-CoV-2 by Computational Approach. *J. Infect. Public Health* **2022**, *15*, 1180–1191, doi:10.1016/j.jiph.2022.09.007.

11. Sivaraman, H.; Er, S.Y.; Choong, Y.K.; Gavor, E.; Sivaraman, J. Structural Basis of SARS-CoV-2- and SARS-CoV-Receptor Binding and Small-Molecule Blockers as Potential Therapeutics. *Annu. Rev. Pharmacol. Toxicol.* **2021**, *61*, 465–493, doi:10.1146/annurev-pharmtox-061220-093932.

12. Bertolin, A.P.; Weissmann, F.; Zeng, J.; Posse, V.; Milligan, J.C.; Canal, B.; Ulferts, R.; Wu, M.; Drury, L.S.; Howell, M.; et al. Identifying SARS-CoV-2 Antiviral Compounds by Screening for Small Molecule Inhibitors of Nsp12/7/8 RNA-Dependent RNA Polymerase. *Biochem. J.* **2021**, *478*, 2425–2443, doi:10.1042/bcj20210200.

13. Baby, K.; Maity, S.; Mehta, C.H.; Suresh, A.; Nayak, U.Y.; Nayak, Y. Targeting SARS-CoV-2 RNA-Dependent RNA Polymerase: An in Silico Drug Repurposing for COVID-19. *F1000Research* **2020**, *9*, 1166, doi:10.12688/f1000research.26359.1.

14. Kirchdoerfer, R.N.; Ward, A.B. Structure of the SARS-CoV Nsp12 Polymerase Bound to Nsp7 and Nsp8 Co-Factors. *Nat. Commun.* **2019**, *10*, 2342, doi:10.1038/s41467-019-10280-3.

15. Ahmad, J.; Ikram, S.; Ahmad, F.; Rehman, I.U.; Mushtaq, M. SARS-CoV-2 RNA Dependent RNA Polymerase (RdRp) – A Drug Repurposing Study. *Heliyon* **2020**, *6*, e04502, doi:10.1016/j.heliyon.2020.e04502.

16. El Sohaimy, S.; Abdo, N.; Shehata, M.; Moheyeldin, O. Inhibition of COVID-19 RNA-Dependent RNA Polymerase by Natural Bioactive Compounds: Molecular Docking Analysis. *Egypt. J. Chem.* **2021**, *64*, 1989–2001, doi:10.21608/ejchem.2021.45739.2947.

17. McDonald, E.G.; Lee, T.C. Nirmatrelvir-Ritonavir for COVID-19. *CMAJ* **2022**, *194*, E218, doi:10.1503/cmaj.220081.

18. U.S. Food and Drug Administration (FDA) FDA Approves First Oral Antiviral for Treatment of COVID-19 in Adults Available online: https://www.fda.gov/news-events/press-announcements/fda-approves-first-oral-antiviral-treatment-covid-19-adults (accessed on 6 November 2023).

19. Jayk Bernal, A.; Gomes da Silva, M.M.; Musungaie, D.B.; Kovalchuk, E.; Gonzalez, A.; Delos Reyes, V.; Martín-Quirós, A.; Caraco, Y.; Williams-Diaz, A.; Brown, M.L.; et al. Molnupiravir for Oral Treatment of Covid-19 in Nonhospitalized Patients. *N. Engl. J. Med.* **2022**, *386*, 509–520, doi:10.1056/nejmoa2116044.

20. Manabe, T.; Kambayashi, D.; Akatsu, H.; Kudo, K. Favipiravir for the Treatment of Patients with COVID-19: A Systematic Review and Meta-Analysis. *BMC Infect. Dis.* **2021**, *21*, 489, doi:10.1186/s12879-021-06164-x.

21. McAuley, A.J.; Jansen van Vuren, P.; Mohammed, M.-U.-R.; Faheem; Goldie, S.; Riddell, S.; Gödde, N.J.; Styles, I.K.; Bruce, M.P.; Chahal, S.; et al. Use of Human Lung Tissue Models for Screening of Drugs against SARS-CoV-2 Infection. *Viruses* **2022**, *14*, 2417, doi:10.3390/v14112417.

22. Reis, G.; dos Santos Moreira-Silva, E.A.; Silva, D.C.M.; Thabane, L.; Milagres, A.C.; Ferreira, T.S.; dos Santos, C.V.Q.; de Souza Campos, V.H.; Nogueira, A.M.R.; de Almeida, A.P.F.G.; et al. Effect of Early Treatment with Fluvoxamine on Risk of Emergency Care and Hospitalisation among Patients with COVID-19: The TOGETHER Randomised, Platform Clinical Trial. *Lancet Glob. Heal.* **2022**, *10*, e42–e51, doi:10.1016/S2214-109X(21)00448-4.

23. Butler, C.C.; Hobbs, F.D.R.; Gbinigie, O.A.; Rahman, N.M.; Hayward, G.; Richards, D.B.; Dorward, J.; Lowe, D.M.; Standing, J.F.; Breuer, J.; et al. Molnupiravir plus Usual Care versus Usual Care Alone as Early Treatment for Adults with COVID-19 at Increased Risk of Adverse Outcomes (PANORAMIC): An Open-Label, Platform-Adaptive Randomised Controlled Trial. *Lancet* **2023**, *401*, 281–293, doi:10.1016/S0140-6736(22)02597-1.

24. Wise, J. Covid-19: Molnupiravir Does Not Cut Hospital Admissions or Deaths in Vaccinated People at High Risk, Trial Finds. *BMJ* **2022**, o3055, doi:10.1136/bmj.o3055.

25. Kozlov, M. Merck's COVID Pill Loses Its Lustre: What That Means for the Pandemic. *Nature* **2021**, doi:10.1038/d41586-021-03667-0.

26. Batool, S.; Vuthaluru, K.; Hassan, A.; Bseiso, O.; Tehseen, Z.; Pizzorno, G.; Rodriguez Reyes, Y.; Saleem, F. Efficacy and Safety of Favipiravir in Treating COVID-19 Patients: A Meta-Analysis of Randomized Control Trials. *Cureus* **2023**, *15*, e33676, doi:10.7759/cureus.33676.

27. Bosaeed, M.; Alharbi, A.; Mahmoud, E.; Alrehily, S.; Bahlaq, M.; Gaifer, Z.; Alturkistani, H.; Alhagan, K.; Alshahrani, S.; Tolbah, A.; et al. Efficacy of Favipiravir in Adults with Mild COVID-19: A Randomized, Double-Blind, Multicentre, Placebo-Controlled Clinical Trial. *Clin. Microbiol. Infect.* **2022**, *28*, 602–608, doi:10.1016/j.cmi.2021.12.026.

28. Shah, P.L.; Orton, C.M.; Grinsztejn, B.; Donaldson, G.C.; Crabtree Ramírez, B.; Tonkin, J.; Santos, B.R.; Cardoso, S.W.; Ritchie, A.I.; Conway, F.; et al. Favipiravir in Patients Hospitalised with COVID-19 (PIONEER Trial): A Multicentre, Open-Label, Phase 3, Randomised Controlled Trial of Early Intervention versus Standard Care. *Lancet Respir. Med.* **2023**, *11*, 415–424, doi:10.1016/S2213-2600(22)00412-X.

29. Siripongboonsitti, T.; Ungtrakul, T.; Tawinprai, K.; Nimmol, T.; Buttakosa, M.; Sornsamdang, G.; Jarrusrojwuttikul, T.; Silapant, P.; Mahanonda, N. Efficacy of Combination Therapy of Fluvoxamine and Favipiravir vs Favipiravir Monotherapy to Prevent Severe COVID-19 among Mild to Moderate COVID-19 Patients: Open-Label Randomized Controlled Trial (EFFaCo Study). *Int. J. Infect. Dis.* **2023**, *134*, 211–219, doi:10.1016/j.ijid.2023.06.018.

30. Lenze, E.J.; Mattar, C.; Zorumski, C.F.; Stevens, A.; Schweiger, J.; Nicol, G.E.; Miller, J.P.; Yang, L.; Yingling, M.; Avidan, M.S.; et al. Fluvoxamine vs Placebo and Clinical Deterioration in Outpatients With Symptomatic COVID-19. *JAMA* **2020**, *324*, 2292, doi:10.1001/jama.2020.22760.

31. Calusic, M.; Marcec, R.; Luksa, L.; Jurkovic, I.; Kovac, N.; Mihaljevic, S.; Likic, R. Safety and Efficacy of Fluvoxamine in COVID-19 ICU Patients: An Open Label, Prospective Cohort Trial with Matched Controls. *Br. J. Clin. Pharmacol.* **2022**, *88*, 2065–2073, doi:10.1111/bcp.15126.

32. Muzaffar-Ur-Rehman, M.; Suryakant, C.K.; Chandu, A.; Kumar, B.K.; Joshi, R.P.; Jadav, S.R.; Sankaranarayanan, M.; Vasan, S.S. Molecular Docking and Dynamics Identify Potential Drugs to Be Repurposed as SARS-CoV-2 Inhibitors. *J. Comput. Biophys. Chem.* **2023**, 1–23, doi:10.1142/s2737416523500552.

33. Zamzami, M.A. Molecular Docking, Molecular Dynamics Simulation and MM-GBSA Studies of the Activity of Glycyrrhizin Relevant Substructures on SARS-CoV-2 RNA-Dependent-RNA Polymerase. *J. Biomol. Struct. Dyn.* **2023**, *41*, 1846–1858, doi:10.1080/07391102.2021.2025147.

34. Brunt, D.; Lakernick, P.M.; Wu, C. Discovering New Potential Inhibitors to SARS-CoV-2 RNA Dependent RNA Polymerase (RdRp) Using High Throughput Virtual Screening and Molecular Dynamics Simulations. *Sci. Rep.* **2022**, *12*, 19986, doi:10.1038/s41598-022-24695-4.

35. Lu, J.; Lu, W.; Jiang, H.; Yang, C.; Dong, X. Molecular Docking and Dynamics of Phytochemicals From Chinese Herbs With SARS-CoV-2 RdRp. *Nat. Prod. Commun.* **2022**, *17*, 1934578X2211056, doi:10.1177/1934578X221105693.

36. Askari, F.S.; Ebrahimi, M.; Parhiz, J.; Hassanpour, M.; Mohebbi, A.; Mirshafiey, A. Digging for the Discovery of SARS-CoV-2 Nsp12 Inhibitors: A Pharmacophore-Based and Molecular Dynamics Simulation Study. *Future Virol.* **2022**, *17*, 743–759, doi:10.2217/fvl-2022-0054.

37. Uengwetwanit, T.; Chutiwitoonchai, N.; Wichapong, K.; Karoonuthaisiri, N. Identification of Novel SARS-CoV-2 RNA Dependent RNA Polymerase (RdRp) Inhibitors: From in Silico Screening to Experimentally Validated Inhibitory Activity. *Comput. Struct. Biotechnol. J.* **2022**, *20*, 882–890, doi:10.1016/j.csbj.2022.02.001.

38. Chinnamadhu, A.; Ramakrishnan, J.; Suresh, S.; Ramadurai, P.; Poomani, K. Dynamics and Binding Affinity of Nucleoside and Non-Nucleoside Inhibitors with RdRp of SARS-CoV-2: A Molecular Screening, Docking, and Molecular Dynamics Simulation Study. *J. Biomol. Struct. Dyn.* **2022**, 1–15, doi:10.1080/07391102.2022.2154844.

39. Alzahrani, F.A.; Alkarim, S.A.; Hawsawi, Y.M.; Abdulaal, W.H.; Albiheyri, R.; Kurdi, B.; Alguridi, H.; El-Magd, M.A. 25 (S)-Hydroxycholesterol Acts as a Possible Dual Enzymatic Inhibitor of SARS-CoV-2 M pro and RdRp–: An Insight from Molecular Docking and Dynamics Simulation Approaches. *J. Biomol. Struct. Dyn.* **2023**, *41*, 4744–4755, doi:10.1080/07391102.2022.2072392.

40. Alexpandi, R.; De Mesquita, J.F.; Pandian, S.K.; Ravi, A.V. Quinolines-Based SARS-CoV-2 3CLpro and RdRp Inhibitors and Spike-RBD-ACE2 Inhibitor for Drug-Repurposing Against COVID-19: An in Silico Analysis. *Front. Microbiol.* **2020**, *11*, 1796, doi:10.3389/fmicb.2020.01796.

41. Kushwaha, P.P.; Singh, A.K.; Bansal, T.; Yadav, A.; Prajapati, K.S.; Shuaib, M.; Kumar, S. Identification of Natural Inhibitors Against SARS-CoV-2 Drugable Targets Using Molecular Docking, Molecular Dynamics Simulation, and MM-PBSA Approach. *Front. Cell. Infect. Microbiol.* **2021**, *11*, 730288, doi:10.3389/fcimb.2021.730288.

42. Shady, N.H.; Hayallah, A.M.; Mohamed, M.F.A.; Ghoneim, M.M.; Chilingaryan, G.; Al-Sanea, M.M.; Fouad, M.A.; Kamel, M.S.; Abdelmohsen, U.R. Targeting 3CLpro and SARS-CoV-2 RdRp by Amphimedon Sp. Metabolites: A Computational Study. *Molecules* **2021**, *26*, 3775, doi:10.3390/molecules26123775.

43. Gajjar, N.D.; Dhameliya, T.M.; Shah, G.B. In Search of RdRp and Mpro Inhibitors against SARS CoV-2: Molecular Docking, Molecular Dynamic Simulations and ADMET Analysis. *J. Mol. Struct.* **2021**, *1239*, 130488, doi:10.1016/j.molstruc.2021.130488.

44. Parihar, A.; Sonia, Z.F.; Akter, F.; Ali, M.A.; Hakim, F.T.; Hossain, M.S. Phytochemicals-Based Targeting RdRp and Main Protease of SARS-CoV-2 Using Docking and Steered Molecular Dynamic Simulation: A Promising Therapeutic Approach for Tackling COVID-19. *Comput. Biol. Med.* **2022**, *145*, 105468, doi:10.1016/j.compbiomed.2022.105468.

45. M A Kawsar, S.; Hosen, M.A.; Ahmad, S.; El Bakri, Y.; Laaroussi, H.; Ben Hadda, T.; Almalki, F.A.; Ozeki, Y.; Goumri-Said, S. Potential SARS-CoV-2 RdRp Inhibitors of Cytidine Derivatives: Molecular Docking, Molecular Dynamic Simulations, ADMET, and POM Analyses for the Identification of Pharmacophore Sites. *PLoS One* **2022**, *17*, e0273256, doi:10.1371/journal.pone.0273256.

46. Veerasamy, R.; Karunakaran, R. Molecular Docking Unveils the Potential of Andrographolide Derivatives against COVID-19: An in Silico Approach. *J. Genet. Eng. Biotechnol.* **2022**, *20*, 58, doi:10.1186/s43141-022-00339-y.

47. Gangadharan, S.; Ambrose, J.M.; Rajajagadeesan, A.; Kullappan, M.; Patil, S.; Gandhamaneni, S.H.; Veeraraghavan, V.P.; Nakkella, A.K.; Agarwal, A.; Jayaraman, S.; et al. Repurposing of Potential Antiviral Drugs against RNA-Dependent RNA Polymerase of SARS-CoV-2 by Computational Approach. *J. Infect. Public Health* **2022**, *15*, 1180–1191, doi:10.1016/j.jiph.2022.09.007.

48. Jang, W.D.; Jeon, S.; Kim, S.; Lee, S.Y. Drugs Repurposed for COVID-19 by Virtual Screening of 6,218 Drugs and Cell-Based Assay. *Proc. Natl. Acad. Sci. U. S. A.* **2021**, *118*, e2024302118, doi:10.1073/pnas.2024302118.

49. Hosseini, M.; Chen, W.; Xiao, D.; Wang, C. Computational Molecular Docking and Virtual Screening Revealed Promising SARS-CoV-2 Drugs. *Precis. Clin. Med.* **2021**, *4*, 1–16, doi:10.1093/pcmedi/pbab001.

50. El Hassab, M.A.; Hemeda, L.R.; Elsayed, Z.M.; Al-Rashood, S.T.; Abdel-Hamid Amin, M.K.; Abdel-Aziz, H.A.; Eldehna, W.M. Computational Prediction of the Potential Target of SARS-CoV-2 Inhibitor Plitidepsin via Molecular Docking, Dynamic Simulations and MM-PBSA Calculations. *Chem. Biodivers.* **2022**, *19*, e202100719, doi:10.1002/cbdv.202100719.

51. Vesga, L.C.; Ruiz-Hernández, C.A.; Alvarez-Jacome, J.J.; Duque, J.E.; Rincon-Orozco, B.; Mendez-Sanchez, S.C. Repurposing of Four Drugs as Anti-SARS-CoV-2 Agents and Their Interactions with Protein Targets. *Sci. Pharm.* **2022**, *90*, 24, doi:10.3390/scipharm90020024.

52. Elfiky, A.A. Dual Targeting of RdRps of SARS-CoV-2 and the Mucormycosis-Causing Fungus: An in Silico Perspective. *Future Microbiol.* **2022**, *17*, 755–762, doi:10.2217/fmb-2022-0083.

53. Mohammed, A.O.; Abo-Idrees, M.I.; Makki, A.A.; Ibraheem, W.; Alzain, A.A. Drug Repurposing against Main Protease and RNA-Dependent RNA Polymerase of SARS-CoV-2 Using Molecular Docking, MM-GBSA Calculations and Molecular Dynamics. *Struct. Chem.* **2022**, *33*, 1553–1567, doi:10.1007/s11224-022-01999-9.

54. Ribaudo, G.; Ongaro, A.; Oselladore, E.; Zagotto, G.; Memo, M.; Gianoncelli, A. A Computational Approach to Drug Repurposing against SARS-CoV-2 RNA Dependent RNA Polymerase (RdRp). *J. Biomol. Struct. Dyn.* **2022**, *40*, 1101–1108, doi:10.1080/07391102.2020.1822209.

55. Thompson, J.; Wang, Y.; Dreischulte, T.; Barreiro, O.; Gonzalez, R.J.; Hanč, P.; Matysiak, C.; Neely, H.R.; Rottenkolber, M.; Haskell, T.; et al. Association between Bisphosphonate Use and COVID-19 Related Outcomes. *Elife* **2023**, *12*, e79548, doi:10.7554/eLife.79548.

56. Wang, B.; Svetlov, D.; Artsimovitch, I. NMPylation and De-NMPylation of SARS-CoV-2 Nsp9 by the NiRAN Domain. *Nucleic Acids Res.* **2021**, *49*, 8822–8835, doi:10.1093/nar/gkab677.

57. Drake, M.T.; Clarke, B.L.; Khosla, S. Bisphosphonates: Mechanism of Action and Role in Clinical Practice. *Mayo Clin. Proc.* **2008**, *83*, 1032–1045, doi:10.4065/83.9.1032.

58. Kunzmann, V.; Bauer, E.; Feurle, J.; Tony Florian Weißinger, H.-P.; Wilhelm, M.; Tony, Florian Weißinger, H.-P.; Wilhelm, M. Stimulation of Γδ T Cells by Aminobisphosphonates and Induction of Antiplasma Cell Activity in Multiple Myeloma. *Blood* **2000**, *96*, 384–392, doi:10.1182/blood.V96.2.384.

59. Davies, M.; Nowotka, M.; Papadatos, G.; Dedman, N.; Gaulton, A.; Atkinson, F.; Bellis, L.; Overington, J.P. ChEMBL Web Services: Streamlining Access to Drug Discovery Data and Utilities. *Nucleic Acids Res.* **2015**, *43*, W612-20, doi:10.1093/nar/gkv352.

60. Friesner, R.A.; Banks, J.L.; Murphy, R.B.; Halgren, T.A.; Klicic, J.J.; Mainz, D.T.; Repasky, M.P.; Knoll, E.H.; Shelley, M.; Perry, J.K.; et al. Glide: A New Approach for Rapid, Accurate Docking and Scoring. 1. Method and Assessment of Docking Accuracy. *J. Med. Chem.* **2004**, *47*, 1739–1749, doi:10.1021/jm0306430.

61. Shelley, J.C.; Cholleti, A.; Frye, L.L.; Greenwood, J.R.; Timlin, M.R.; Uchimaya, M. Epik: A Software Program for PK(a) Prediction and Protonation State Generation for Drug-like Molecules. *J. Comput. Aided. Mol. Des.* **2007**, *21*, 681–691, doi:10.1007/s10822-007-9133-z.

62. Koulgi, S.; Jani, V.; Uppuladinne, M.V.N.; Sonavane, U.; Joshi, R. Remdesivir-Bound and Ligand-Free Simulations Reveal the Probable Mechanism of Inhibiting the RNA Dependent RNA Polymerase of Severe Acute Respiratory Syndrome Coronavirus 2. *RSC Adv.* **2020**, *10*, 26792–26803, doi:10.1039/D0RA04743K.

63. Veber, D.F.; Johnson, S.R.; Cheng, H.-Y.; Smith, B.R.; Ward, K.W.; Kopple, K.D. Molecular Properties That Influence the Oral Bioavailability of Drug Candidates. *J. Med. Chem.* **2002**, *45*, 2615–2623, doi:10.1021/jm020017n.

64. Halgren, T.A.; Murphy, R.B.; Friesner, R.A.; Beard, H.S.; Frye, L.L.; Pollard, W.T.; Banks, J.L. Glide: A New Approach for Rapid, Accurate Docking and Scoring. 2. Enrichment Factors in Database Screening. *J. Med. Chem.* **2004**, *47*, 1750–1759, doi:10.1021/jm030644s.

65. Genheden, S.; Ryde, U. The MM/PBSA and MM/GBSA Methods to Estimate Ligand-Binding Affinities. *Expert Opin. Drug Discov.* **2015**, *10*, 449–461, doi:10.1517/17460441.2015.1032936.

66. Karplus, M.; McCammon, J.A. Molecular Dynamics Simulations of Biomolecules. *Nat. Struct. Biol.* **2002**, *9*, 646–652, doi:10.1038/nsb0902-646.

67. Mark, P.; Nilsson, L. Structure and Dynamics of the TIP3P, SPC, and SPC/E Water Models at 298 K. *J. Phys. Chem. A* **2001**, *105*, 9954–9960, doi:10.1021/jp003020w.

68. Valdés-Tresanco, M.S.; Valdés-Tresanco, M.E.; Valiente, P.A.; Moreno, E. Gmx_MMPBSA: A New Tool to Perform End-State Free Energy Calculations with GROMACS. *J. Chem. Theory Comput.* **2021**, *17*, 6281–6291, doi:10.1021/acs.jctc.1c00645.

69. Miller, B.R.; McGee, T.D.; Swails, J.M.; Homeyer, N.; Gohlke, H.; Roitberg, A.E. MMPBSA.Py : An Efficient Program for End-State Free Energy Calculations. *J. Chem. Theory Comput.* **2012**, *8*, 3314–3321, doi:10.1021/ct300418h.

70. Duan, L.; Liu, X.; Zhang, J.Z.H. Interaction Entropy: A New Paradigm for Highly Efficient and Reliable Computation of Protein-Ligand Binding Free Energy. *J. Am. Chem. Soc.* **2016**, *138*, 5722–5728, doi:10.1021/jacs.6b02682.

71. Shirts, M.R.; Klein, C.; Swails, J.M.; Yin, J.; Gilson, M.K.; Mobley, D.L.; Case, D.A.; Zhong, E.D. Lessons Learned from Comparing Molecular Dynamics Engines on the SAMPL5 Dataset. *J. Comput. Aided. Mol. Des.* **2017**, *31*, 147–161, doi:10.1007/s10822-016-9977-1.

72. Ekberg, V.; Ryde, U. On the Use of Interaction Entropy and Related Methods to Estimate Binding Entropies. *J. Chem. Theory Comput.* **2021**, *17*, 5379–5391, doi:10.1021/acs.jctc.1c00374.

73. Dutta, K.; Shityakov, S.; Morozova, O.; Khalifa, I.; Zhang, J.; Zhu, W.; Panda, A.; Ghosh, C. Beclabuvir Can Inhibit the RNA-Dependent RNA Polymerase of Newly Emerged Novel Coronavirus (SARS-CoV-2). *Preprint* **2020**, doi:10.20944/preprints202003.0395.v2.

74. Homeyer, N.; Gohlke, H. Free Energy Calculations by the Molecular Mechanics Poisson–Boltzmann Surface Area Method. *Mol. Inform.* **2012**, *31*, 114–122, doi:10.1002/minf.201100135.

75. Cervelli, M.J.; Russ, G.R. Principles of Drug Therapy, Dosing, and Prescribing in Chronic Kidney Disease and Renal Replacement Therapy. In *Comprehensive Clinical Nephrology*; Elsevier, 2010; pp. 871–893 ISBN 9780323077668.